AIAA 99-0304

Experimental Measurement of Venturi Discharge Coefficient Including Sensitivity to Geometric and Flow Quality Variables

D. K. Beale
Sverdrup Technology, Inc., AEDC Group
Arnold Engineering Development Center
Arnold Air Force Base, Tennessee 37389

37th AIAA Aerospace Sciences Meeting & Exhibit
January 11-14, 1999 / Reno, NV

Experimental Measurement of Venturi Discharge Coefficient Including Sensitivity to Geometric and Flow Quality Variables*

D. K. Beale†
Sverdrup Technology, Inc., AEDC Group
Arnold Engineering Development Center
Arnold Air Force Base, TN 37389

Abstract

The Arnold Engineering Development Center (AEDC) initiated an airflow measurement technique investigation to address turbine engine test requirements with respect to both airflow measurement accuracy and costs. The effort encompassed development of a research test cell to serve as an airflow calibration facility and testing of a series of venturi models. The experiments included a repeat of experiments conducted in 1961 that form the basis for the Engine Test Facility (ETF) critical flow venturi flow coefficients. The tests provided a verification of the original measurements substantiating the current AEDC flow coefficients. In addition, the experiments included a parametric investigation of venturi flow coefficient sensitivities to flow quality, geometric, and installation parameters. These sensitivities provided information for evaluating airflow measurement accuracy provided by venturis installed in ETF test facilities.

Nomenclature

Ae	Venturi exit area, sq in.
Ai	Venturi inlet plane area, sq in.
At	Venturi throat cross-sectional area, sq in.
Cd	Venturi discharge coefficient or flow coefficient
CF DEV	Absolute value of deviation in CFBA-1 between test case with perturbed parameters and baseline normalized by the baseline.
Dpl	Plenum chamber diameter, in.
Dt	Venturi throat diameter, in.
Fn	Net thrust, lbf
Fs	Scale force, lbf
MACH	Local Mach number in the venturi core flow based on local static pressure and inlet total pressure
Pa	Ambient pressure, psia
Ps	Static pressure, psia
PT	Local total pressure in the boundary layer, psia
PTINF	Free-stream total pressure as measured in the plenum chamber, psia
REY	Venturi throat Reynolds number. Reynolds number based on throat flow conditions and throat diameter.
RHO	Density, lbm/cubic ft
Rt	Venturi throat radius, in.
TT	Total temperature as measured in plenum, R
V	Velocity, ft/sec
VINF	Free-stream velocity
W	Actual airflow rate, lbm/sec
WI	Indicated or ideal airflow rate, lbm/sec
Xb	Spacing between the venturi inlet plane and the bulkhead, in.
Y	Boundary layer total pressure probe immersion. Distance from venturi wall to center of total pressure probe opening, in.
YI	Spacing between the venturi lip and the wall of the plenum chamber

* The research reported herein was performed by the Arnold Engineering Development Center (AEDC), Air Force Materiel Command. Work and analysis for this research were performed by personnel of Sverdrup Technology, Inc., AEDC Group, technical services contractor for AEDC. Further reproduction is authorized to satisfy needs of the U. S. Government.

† Senior Member, AIAA.

Subscripts

1 Engine inlet

Introduction

Turbine engine ground test facilities provide the aircraft system developer the means to evaluate propulsion system configurations at various stages of the vehicle development and deployment cycle. Early in the development of a new system, the ground test facilities furnish the information necessary to help ensure that the design process converges to a vehicle that meets the mission objectives. In this role, the turbine engine test facility helps predict the performance, operability, and durability of an integrated airframe-inlet-engine nozzle system enabling the designer to make valid design decisions prior to prototyping. Performance encompasses such parameters as turbine engine thrust and fuel consumption which, in turn, influence the entire spectrum of aircraft performance including takeoff, maneuvers, fuel consumption/ range, and landing. Operability involves such parameters as engine surge margin when subjected to the distorted flow developed by the airframe and inlet. Durability involves evaluations of the structural integrity of the system components.

As the vehicle development cycle progresses, the turbine engine test facility provides performance, operability, and durability information necessary to refine the design and prevent shortfalls in the fielded system. Following the fielding of a system, the ground test facility continues to serve in the development of system upgrades and in the resolution of problems that may arise. In each case, the task of the turbine engine test cell centers on providing the needed simulation fidelity early enough to reduce the overall system development costs and risks.

The simulation fidelity required by the turbine engine test cell depends to a large extent on the objectives of the particular evaluation. Performance tests and operability tests inherently emphasize different parameters. Likewise, different types of aircraft may emphasize somewhat different parameters. For example, a transport aircraft designer may focus primarily on fuel consumption and range while a fighter aircraft designer may focus on avoiding surge during the rigors of combat maneuvering. Thus, the class of aircraft system, the particular evaluation objectives, and the maturity of the system affect the parameters of interest and the fidelity required. However, common to most turbine engine ground tests is the requirement to quantify the engine airflow rate accurately. With respect to airflow rate, the variation in aircraft systems and test requirements may translate to variations in airflow accuracy requirements.

The Arnold Engineering Development Center (AEDC) provides the services of a number of turbine engine test cells to meet a variety of needs. During the past decade, the AEDC test mission with respect to turbine engine testing has encompassed both fighter aircraft propulsion systems and transport aircraft propulsion systems. As a result, the fidelity in the airflow measurements and the need to reduce the costs associated with those measurements have become key elements in the AEDC technology investment strategy.

The goal of this paper is to present the test community an initiative underway at AEDC focused on improving the airflow measurement state of the art. The objectives of the improvement initiative center on verifying airflow measurement accuracy, developing methods for improving accuracy, and developing alternative airflow measurement techniques offering the potential for substantial test cost reductions. The presentation in the following sections begins with a summary of the airflow measurement methodologies, defining the apparatus and measurements used in typical turbine engine tests. Subsequent sections describe an investigation of a number of parameters liable to affect airflow measurement accuracy. These include venturi geometry, apparatus installation, and flow quality parameters. The paper concludes with a mention of the plans for future work focused on the alternative airflow measurement techniques.

Airflow Measurement in Direct-Connect Turbine Engine Tests

An appreciation for the role that airflow rate assumes in the evaluation of turbine engines in ground test facilities may be realized through examination of the equations for thrust. Refer-

ences 1 and 2 summarize methods of determining turbine engine thrust during ground tests. A commonly used method, called the scale force method, applies force measurements provided by an external balance. This so called scale force measurement, in conjunction with pressure-area and momentum force components, provides the gross and net thrust. Reference 1 provides the equations describing gross thrust and net thrust, as well as the influences of various parameters on the uncertainty in thrust. The equation for the net thrust is of the form:

$$Fn = W_1V_1 + A_1(Ps_1\text{-}Pa) + Fs - W_1VINF$$

As a result, W affects the net thrust through an influence coefficient of the form:

$$\frac{\partial Fn}{\partial W}$$

The airflow rate accuracy has a significant effect on thrust measurement accuracy. The influence coefficients presented in Refs. 1 and 2 show that a 1-percent error in the airflow rate measurement may yield a 0.3-percent error in the thrust determination. Thus, a 0.4- to 0.5-percent airflow measurement error, typical of current tests, may yield a 0.1- or 0.2-percent thrust measurement error. The influence of the airflow rate measurement on thrust propagates to the turbine engine performance assessment and ultimately to the evaluation of the flight vehicle performance. Therefore, the fidelity in airflow measurements becomes a key consideration in the ground test evaluation.

The direct-connect test serves as the mainstay of turbine engine tests in the AEDC altitude test facilities. The methodology earns its name from an installation characterized by a direct connection between turbine engine and air supply duct, as shown schematically in Fig. 1. A bellmouth provides the transition from the test cell plenum to the engine air supply duct. The air supply duct diameter matches the engine face diameter and so is unique to the particular test. A thrust stand typically supports the engine in the test cell and provides the scale force measurements. The engine exhaust enters a diffuser, which uses the flow momentum to augment test facility exhaust plant pumping.

The simulation of the flight environment in the direct-connect test is based on establishing conditions of Mach number, pressure, and temperature in the air supply duct equal to the conditions delivered to the engine face by the aircraft inlet diffuser duct. For example, the simulation of a fighter aircraft at supersonic conditions generally entails the establishment of the corresponding subsonic conditions that exist following the deceleration and pressure recovery processes of the aircraft inlet system. By establishing the altitude pressure conditions in the test section, the methodology simulates flight conditions at the nozzle exit. However, the simulation neglects the external flow over the nozzle.

The direct-connect method provides the means to evaluate turbine engine operability, as well as performance. Operability tests employ screens or other devices mounted forward of the engine in the air supply duct to subject the engine to distorted flows similar to those delivered by the inlet. The latter are often determined in wind tunnel tests.

The direct-connect test installation generally includes provisions for measuring airflow rate as required for the determination of performance parameters such as thrust. The AEDC turbine engine test facilities generally use critical flow venturis, essentially choked converging-diverging noz-

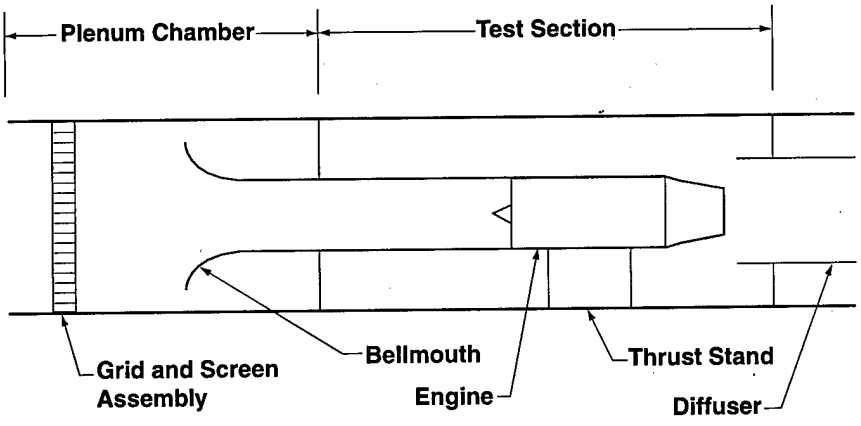

Fig. 1. Turbine engine direct-connect test method.

zles, to relate measurements of total pressure and total temperature to airflow rate. A typical venturi installation in a direct-connect test appears in Fig. 2a. In such an installation, the venturi is mounted upstream of the test cell plenum in the air supply duct. The plenum, containing a flow-straightening grid, establishes uniform conditions at the entrance of the bellmouth feeding the engine air supply duct.

Although a single venturi may be employed as shown in Fig. 2a, a number of facilities use an array of venturis as shown in Fig. 2b. The use of a venturi array permits the optimization of effective venturi area commensurate with the particular test flow rate requirements. Thus, the number of venturis activated for a given test may be tailored to allow sizing of the overall venturi throat area.

The critical flow venturi provides a method of deriving airflow rate from the measurement of fundamental test parameters. In the ideal case, the mass flow through the throat is simply the product of airflow density, throat area, and airflow velocity. If sonic conditions exist at the throat, the ideal airflow rate can be calculated from measurements of the throat area and the upstream stagnation conditions. For air with a specific heat ratio of 1.4, the ideal airflow through a choked venturi is simply:

$$W = 0.5318 \frac{PTINF\ At}{\sqrt{TT}}$$

Instrumentation rakes distributed over the cross section of the venturi air supply duct sense the stagnation conditions of total pressure and total temperature. Venturi operation with subsonic throat conditions requires additional measurements of throat static pressure to define the velocity. The avoidance of the added uncertainty introduced by such measurements motivates the careful sizing of venturi or the tailoring of the venturi array to maintain sonic throat conditions.

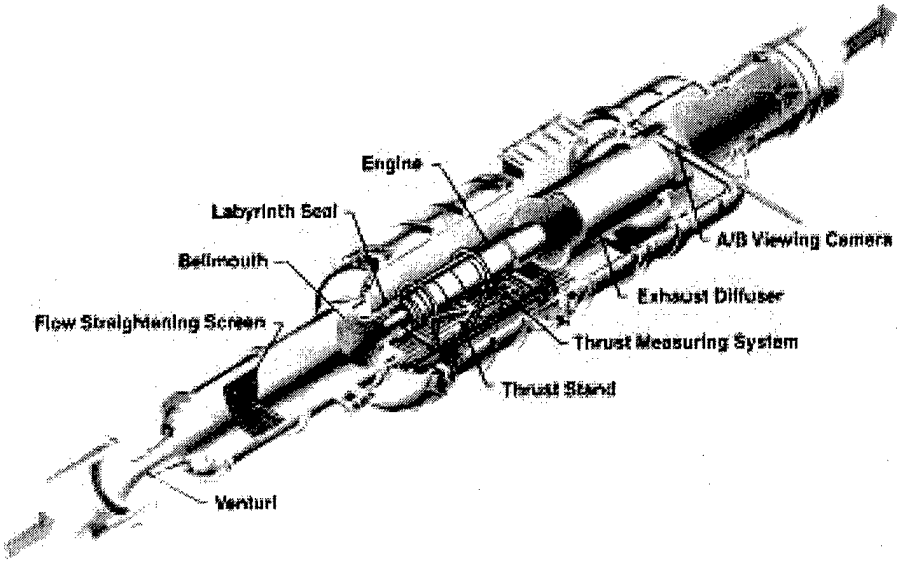

a. Single venturi installation

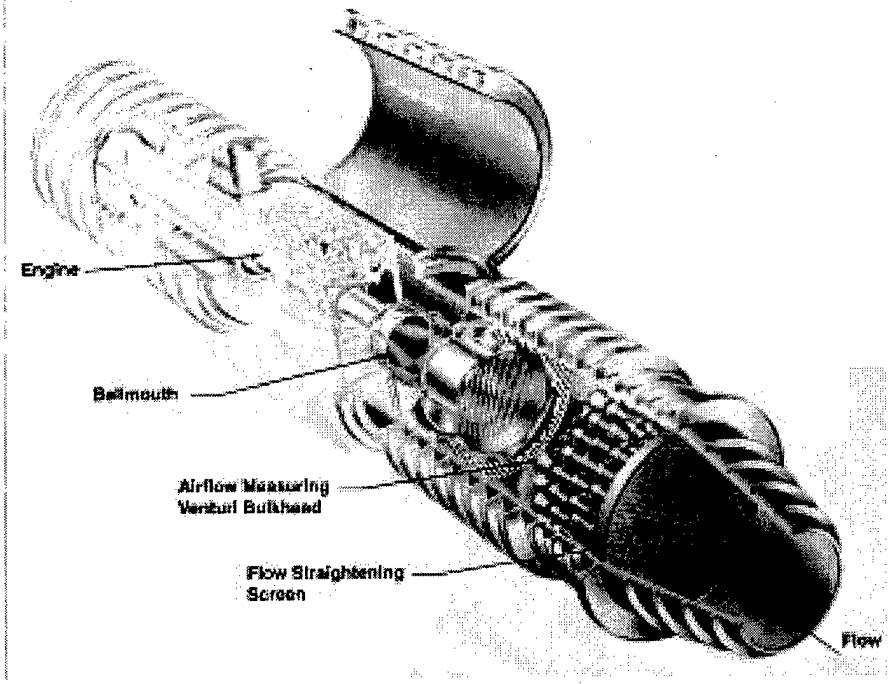

b. Venturi array

Fig. 2. Typical venturi installations in direct-connect Test Facilities.

The ideal calculation of airflow rate assumes uniform flow conditions across the venturi throat translating to a uniform mass flux. In reality, nonuniform conditions exist. Considering the venturi itself, a venturi supplied by uniform conditions, two effects contribute to the nonuniformity. First, viscosity leads to the existence of a boundary-layer along the venturi wall. The viscosity-dominated boundary layer flow yields a variation in velocity from the sonic stream conditions in the core flow to zero at the wall. Thus, a mass flow defect exists in the boundary layer region. The venturi behaves as if a further contraction in area exists at the throat. Secondly, the core flow region outside the relatively thin boundary-layer also fails to achieve the ideal uniform flow conditions. Although viscous effects exert little influence on the core flow, the streamlines are bent by the centrifugal forces experienced by the flow as it curves around the contraction section of the venturi. The streamline curvature yields a radial variation in the Mach number over the throat area and, therefore, a variation in mass flux.

The venturi discharge coefficient, sometimes referred to as the flow coefficient, relates the ideal and the actual venturi flow rates accounting for the nonuniform throat conditions. Specifically, the ideal flow rate multiplied by the flow coefficient yields the actual flow rate. Thus, the flow coefficient consists of a value less than one that must be determined through computational fluid dynamics (CFD) or through a calibration of the venturi. Although a lengthy process may be involved in establishing the flow coefficient, once in hand the flow coefficient simplifies the effort needed to determine the airflow during the engine test. The step from the readily determined ideal airflow rate to the actual airflow rate is reduced to a multiplication:

$$W = (Cd)(WI)$$

The flow coefficient represents the ratio of the actual mass flux integrated over the throat area to the ideal airflow derived assuming uniform throat conditions. Flow coefficients predicted by fully viscous CFD solutions may simply apply the integral of the flow solution mass flux. However, the flow coefficient can also be determined by treating the core and boundar-layer flows separately in a manner analogous to the coupling of boundar-layer solutions and inviscid solutions applied in many external and internal flow analyses. In this case, a viscous solution provides the boundary-layer displacement thickness. The displacement thickness is subtracted from the throat radius to calculate an effective flow area that is lower than the geometric area. The ratio of the effective area to the geometric area yields the viscous component of the flow coefficient. Inviscid solutions of the core flow field provide the streamline curvature characteristics, the nonuniform velocities produced by the centrifugal forces. An integration of the mass flux with the nonuniform core flow velocity distribution in a ratio with the uniform case yields the nonviscous component of the flow coefficient. The product of the two coefficients becomes the overall flow coefficient. The existence of today's powerful viscous CFD codes tends to reinforce the use of the first approach. However, historically the computational state of the art and economy resulted in the use of boundary-layer codes and inviscid core flow codes in the second method.

Experimentally, the flow coefficient may be determined in one of three methods. The first, and perhaps most obvious, is to simply pass a known mass through the venturi while recording the time to yield a flow rate. Normalization by the ideal flow rate yields the flow coefficient. This method has been used for incompressible flow calibrations, using water, for which the mass is easily determined. For compressible flow calibrations using gases, the determination of the mass passed through the venturi requires considerably more effort.

The second method establishes the flow coefficient through direct comparison with a calibration reference, or secondary standard, flow rate-measuring device. In this case, the test venturi to be calibrated is mounted in series with the reference device. The actual flow rate provided by the reference may be normalized by the ideal flow rate determined by the test venturi to yield the flow coefficient. The assumption that the same mass flow passes through both devices demands care in preventing leakage between the devices in the test facility.

The third experimental method applies flowfield probing systems to measure the nonuniform flow conditions in the venturi throat. The resulting distributions in the flow conditions, and, therefore, mass flux, can then be integrated and normalized by the ideal flow rate to produce the flow coefficient. In effect, the procedures described for the CFD flow coefficient are applied substituting flowfield measurements for the computed viscous flow field. In principle, this could be accomplished using traverses of a pitot-static probe and a temperature probe. However, in practice such an approach may lead to insurmountable difficulties. For example, a 5-in.-diam venturi may have a boundary layer less than 0.050-in. thick contributing significantly to the flow coefficient. The difficulties stem from the task of adequately measuring flow profiles in such a small region.

Historically, the probing method overcame the difficulties by applying the approach of separating the flow coefficient into two components as described above. Miniature boundary layer pitot probes provided the total pressure distribution in the viscous region of the flow field. Under the assumption that the static pressure in the boundary-layer remains constant and that the total temperature equates to the plenum stagnation condition, a displacement thickness may be determined and used to quantify the boundary-layer component of the flow coefficient. A traversing static pressure probe or a pitot-static probe provided measurements of the core flow Mach number distribution to quantify the streamline curvature component of the flow coefficient.

The above discussion leads to the expectation that, in the case of a critical flow venturi, the flow coefficient is a function of the Reynolds number and the shape of the venturi contraction section. This is found to be true, at least for the case of a venturi mounted in an infinite plenum so that the venturi alone shapes the flow field. The Reynolds number primarily affects the boundar-layer displacement thickness and, therefore, the viscous component of the flow coefficient. The contraction section shape primarily affects the centrifugal force on the flow field and, therefore, the streamline curvature component. As a result, for a given venturi shape and critical flow conditions, the streamline curvature component is a single value. The viscous component is a function of the Reynolds number.

The accuracy in the airflow measurements provided during a turbine engine test depends on the accuracy of the stagnation condition measurements, accuracy of the venturi throat area measurements, and accuracy in the flow coefficient characterization. The errors in the stagnation condition measurements consist of contributions from the plenum chamber probes/rakes, pressure transducers, thermocouples, data recording system, and data reduction procedures. The error in the throat area depends on the accuracy of the diameter or radius measurements, the density of the measurement grid, and the characterization of throat area variations with respect to the operating environment (pressure and temperature effects). The uncertainty in the flow coefficient depends on the calibration method used and the corresponding stack of experimental errors. As a direct multiplier on the ideal airflow rate, an accurate flow coefficient is pivotal to an accurate airflow rate measurement.

The assertion that the critical flow venturi flow coefficient depends only on Reynolds number and venturi geometry requires the strong supposition that the venturi is sufficiently isolated from the environment that it alone shapes the flow field. In reality, the venturi is always part of a system comprised of finite-sized air supply ducts, bulkheads, manways, instrumentation rakes, and other apparatus. Such features can, in principal, influence the flow coefficient. Furthermore, instrumentation used to define the stagnation conditions becomes part of the system. Instrumentation rakes may directly influence the flow characteristics entering the venturi. During calibration, the measurement errors in the stagnation conditions become part of the flow coefficient errors. For unchoked operation with subsonic throat conditions, throat static pressure instrumentation also becomes part of the system. Static pressure measurements generally prove to be very sensitive to orifice location, orifice design, and orifice imperfections. The historical practice at AEDC has been to operate the venturis with sonic throat conditions to avoid reliance on static pressure measurements, to endeavor to measure stagnation conditions with a fidelity commensurate with

the accuracy sought, and to assume that the variations between the ETF facilities remain consistent with the required accuracy.

An examination of Fig. 2 shows that a considerable variation in the venturi installation exists between the ETF facilities. Figure 2a shows a single venturi forming a spool in the air supply duct. The venturi contraction section physically transitions into the pressure bulkhead. Figure 2b shows an array of much smaller venturis distributed over the pressure bulkhead. Each venturi is "freestanding" in the sense that the contraction section extends upstream into the plenum, in some cases as far as two throat diameters. Furthermore, some of the venturis operate near the plenum centerline while others operate near the plenum wall. In many cases, the venturi array involves groups of venturis operating in very close proximity to each other. Although not shown explicitly, the figures imply that different facilities may exhibit different contraction ratios between the plenum or air supply duct area and effective venturi throat area. Such variations lead to variations in the Mach number of the approaching flow.

In addition to the variation in the installation parameters between facilities, individual venturis may exhibit geometric variations. In some applications, the contraction sections are truncated slightly. In other cases, the aging process degrades surface smoothness as corrosion forms. Finally, all venturis are subject to fabrication tolerances that affect the degree to which a desired contour is achieved.

As each test facility exhibits a uniqueness with respect to the configuration of the air supply system, a variation in the plenum flow quality among the facilities can be anticipated. The upstream ducting, flow mixing systems, flow straightening systems, and plenum subsystems (manways, catwalks, etc.) may contribute to flow nonuniformity and turbulence in the flow delivered to the venturi entrance.

Figure 3 provides a summary of the various parameters that could contribute to the uncertainty in critical flow venturi flow coefficient. They include the installation, geometric, and flow quality parameters. However, they also include the accuracy to which CFD codes used to quantify the flow coefficient model the viscous and inviscid flow conditions. Clearly, the confidence level associated with an airflow measurement accuracy assessment depends substantially on the degree to which the factors presented in Fig. 3 are understood.

It may be apparent at this point that the various installation, geometric, and flow quality parameters interact. Furthermore, many of the installation or geometric effects may influence the venturi flow coefficient by affecting the flow quality at the venturi entrance. The most striking example is contained in the installation features conducive to the formation of the so-called inlet vortex. As explained

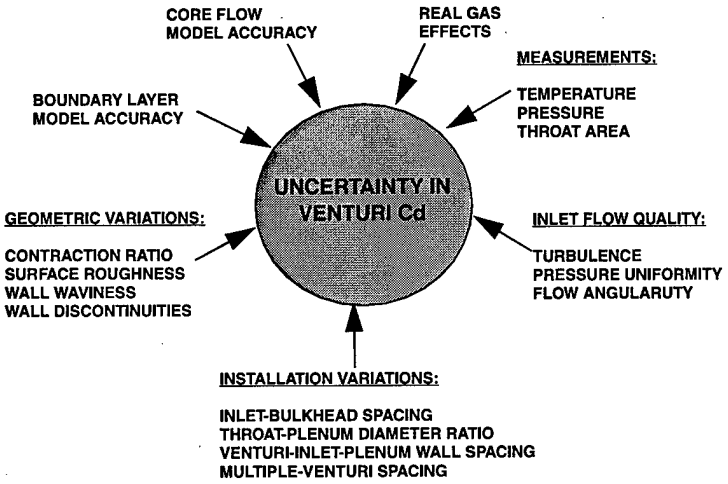

Fig. 3. Parameters contributing to venturi flow coefficient uncertainty.

in Refs. 3 and 4, a freestanding venturi or bellmouth in a plenum provides the environment needed to establish such a vortex, namely upstream vorticity, a flow sink, and a stagnation region for vortex attachment. Thus, to the extent that the venturi flow coefficient is sensitive to swirl, it may be sensitive to the installation parameters such as plenum wall proximity or spacing between venturi inlet plane and the plenum bulkhead.

The discussion presented in this section thus sets the stage for subsequent sections summarizing work currently in progress at AEDC focused on advancing the airflow measurement state of the art.

Description of Airflow Measurement Investigation

The AEDC initiated an extensive airflow measurement technique investigation to address a number of issues relating to the airflow measurement state of the art in the ETF. The issues readily group into three areas, all relating to the use of the critical flow venturi as the facility airflow measurement standard. The first set of issues relates to the validity of venturi flow coefficients, or discharge coefficients, currently applied in the ETF. The second set centers on future airflow measurement accuracy requirements. Finally, the third set of issues involves the substantial test costs associated with current airflow measurement practices.

The first group of issues originated in observations on the part of the AEDC test and evaluation team, as well as AEDC customers, of differences between the ETF flow coefficients and those measured in other facilities. In some cases, differences as high as 0.5 percent were observed, with comparisons showing substantially different trends over certain throat Reynolds number ranges. As a result, AEDC resolved to develop an improved understanding of the critical flow venturi behavior.

The second group of issues, future accuracy requirements, originated in the increased emphasis on fuel consumption and range assessments. The accuracy of aircraft range predictions, derived from direct-connect turbine engine tests, depends on the accuracy of the performance parameters such as thrust. Therefore, due to the influence of airflow rate on performance parameters, the accuracy in range predictions can be traced to airflow measurement accuracy. For transport aircraft applications, engine performance with respect to fuel consumption is a prime consideration and perhaps a deciding factor in the awarding of engine supplier contracts. As a result, AEDC transport engine customers have issued airflow measurement uncertainty goals as low as 0.23 percent, on the order of one-half of typical ETF measurements. Although the accuracy issue first surfaced during tests of large high-bypass engines for transport applications, the fighter aircraft requirements have also elevated the range consideration and the emphasis on airflow measurement accuracy.

The third group of issues, the costs of measuring facility airflow, stems from the constant need to reduce the cost of AEDC test and evaluation services. In recent years, this need has become particularly acute as budgets have dwindled and AEDC competitors have offered alternatives to traditional AEDC customers. The airflow measurement costs originate from four general sources. First, the operation of a choked venturi leads to a total pressure loss that must be overcome by the test facility. This implies either a reduction in the available facility altitude-Mach number envelope or an increase in the plant pumping capacity. The latter translates to more or larger plant machines and more energy costs. The second cost encompasses the manpower and schedule resources needed for installation and removal of the facility venturi(s). In the course of a typical engine test program, the venturis must be installed during the steady-state portion of the engine performance test matrix and removed during the transient tests. As a result, the program must include provisions for a scheduled interrupt and the manhours needed to complete at least one venturi configuration change. Third, sustaining sonic conditions at the venturi throat requires adjustment of the effective venturi throat area according to test conditions. In single-venturi installations, this requires labor and cycle time for removing and replacing venturis. For multiple-venturi installations, this requires test time for activating and deactivating remotely controlled venturis. Finally, remotely controlled venturis incur maintenance costs in the course of ensuring reliability and test readiness.

The three sets of airflow measurement issues translated directly into three overall objectives for this investigation: (1) verify the current AEDC critical flow venturi accuracy of typically 0.4 to 0.5 percent; (2) develop the capability of meeting future airflow measurement accuracy requirements for fuel consumption and range assessments with the customer stated goal of 0.23 percent; and (3) reduce turbine engine test costs and expand the available test envelope commensurate with elimination of the venturi total pressure loss and the elimination of venturi installation, removal, and maintenance procedures.

The approach to accomplishing objective 1 included two general steps. First, the AEDC critical

flow venturi flow coefficient measurements that form the basis for the flow coefficient algorithms currently used in the ETF were verified. This step entailed the repeat and check of experiments conducted in 1961 by Smith and Matz.[5] The second step examined the applicability of the historical database for the current ETF facilities. The applicability issue arose from differences between the current venturi installations and the baseline calibration configuration. Examples of these differences appear in Fig. 3 as surface finish, plenum-to-throat area ratio, venturi inlet-to-bulkhead spacing, venturi-to-plenum wall spacing, and multiple-venturi installations. Furthermore, venturi inlet flow quality issues arose from differences in test cell air supply systems and the use of venturi inlet instrumentation rakes. These deviations introduced the potential for differences between the baseline venturi accuracy and the installed accuracy. Parametric experiments helped quantify the contributions of such deviations to the airflow measurement uncertainty.

The approach to the second objective, currently in progress, centers on reducing venturi flow coefficient errors by accounting for parameters presently neglected in the flow coefficient model. The parameter influence measurements serve to identify the parameters that contribute most significantly to the errors. Depending on the nature of the particular influence, the error is reduced by one of two methods. First, the characterization of the flow coefficient may be improved by incorporating the parameter in the flow coefficient model. Thus, the flow coefficient may be modeled as a function of a number of parameters in addition to the currently used Reynolds number. In cases where the parameter cannot be readily included in the calibration, parameter limitations commensurate with the uncertainty limits will be specified.

The objective 3 effort, also in progress, applies an approach similar to that of objective 2. However, the parametric investigation focuses on developing the unchoked bellmouth as an alternative to the choked venturi as the facility airflow measurement standard. The ultimate goal is to adapt the bellmouth that currently serves as the interface between the facility plenum and the engine air supply duct as the facility airflow measurement standard, eliminating the need for venturi installations.

The approaches described above encompassed both experimentation and computation. Experiments characterized venturi discharge coefficient with respect to dominant geometric, installation, and flow quality variables providing a database for the validation of CFD codes. Computational tools modeled the characteristics and upon validation, will provide flow coefficient algorithms for general application in the ETF facilities.

The extensive number of variables to be considered in the parametric tests resulted in a test matrix composed of five venturis and two bellmouths with eleven overall test configurations. Each of the eleven test configurations, in turn, included a number of "builds" to vary specific test parameters. However, each experiment involved one of two methods of determining flow coefficient. First, the flow-field probe method derived the coefficient from measurements of the throat flow field. The second method derived the coefficient through direct comparison to a calibrated reference venturi.

An existing AEDC research test cell, extensively modified for the airflow measurement investigation, provided the features needed to apply each calibration method. The facility contains two traversing pressure probe systems to support the flow-field survey method and two complete plenum systems for calibrating flowmeters in series with a reference venturi.

In the initial test configurations, two of the venturis were calibrated using the flow-field probe method depicted in Fig. 4a. Measurements of the throat flow field provided the two components of the flow coefficient. Throat boundary-layer total pressure measurements yielded the displacement thickness. A remotely positioned static pressure probe traversed the core flow, providing the Mach number distribution for the streamline curvature component. The venturis calibrated in this fashion served to verify the ETF historical database and as reference venturis for the subsequent experiments.

Following the reference venturi calibrations, the experiments proceeded to the parametric study depicted in Fig. 4b. In each configuration, a test

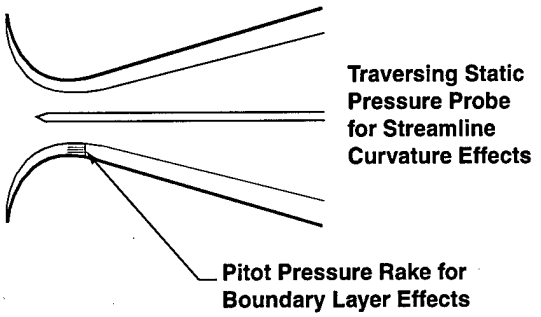

a. Calibration of baseline venturis using flow-field probe method

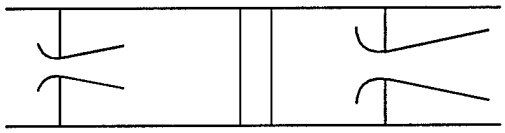

b. Parametric investigation using comparison to calibrated reference venturi

Fig. 4. General experimental approach.

venturi was mounted in series with the reference and subjected to variations in the geometric, installation, and flow quality parameters. Comparisons with the reference venturi provided measures of the variation in flow coefficient due to the variation in test parameters.

Apparatus

Test Facility

The test cell originated as a 15-percent scale model of the ASTF C-2 test cell used in the development and validation of ASTF-related test methods. Under the current initiative, the facility was extensively modified to incorporate the features required in the airflow calibration experiments. The reconfiguration process added a second plenum chamber in series with the existing plenum. Both plenums received flow treatments in the form of porous plates, honeycombs, and screens to ensure uniform plenum flows, as well as instrumentation rakes to sense the plenum flow quality.

In the present configuration, the facility contains a 54-in.-diam upstream plenum, designated plenum A, and a 36-in.-diam downstream plenum, designated plenum B. As shown in Fig. 5, each plenum terminates in a bulkhead, with provisions for mounting up to two venturis or a bellmouth. The selection of two different diameters for the chambers allows for study of plenum-to-venturi (or bellmouth) area ratio effects. Furthermore, the hardware contains provisions for varying installation parameters, including the relative spacing between the venturi or bellmouth inlet lip and the bulkhead, between the lip and the plenum wall, or between the lips of two adjacent venturis for the parametric tests.

In addition to the installation parameters, provisions existed for the introduction of flow nonuniformity of the order expected in full-scale facilities into the plenum B flow. These consisted of a total pressure nonuniformity characteristic of that produced by venturi inlet instrumentation rakes, swirl, and turbulence. Figure 6 illustrates the apparatus used to induce each type of flow condition. A rake geometrically simulating venturi inlet rakes in wide use at the ETF provided the total pressure nonuniformity (Fig. 6a). The tip vortex produced by an airfoil at angle of attack introduced a localized swirl (Fig 6b). A grid of cylindrical bodies introduced turbulence (Fig 6c).

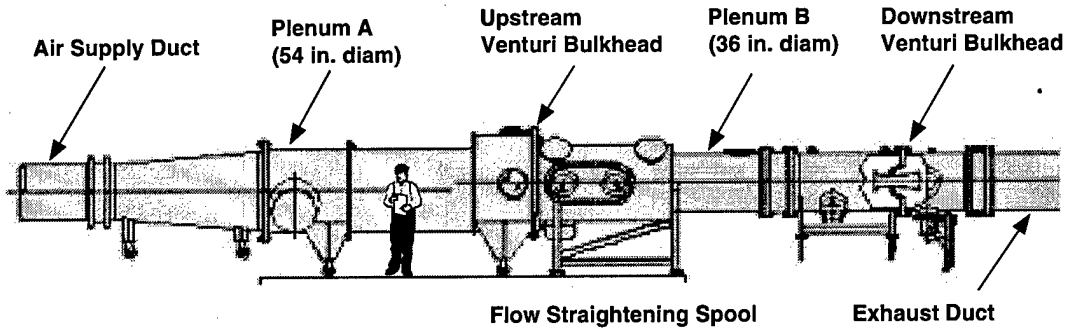

Fig. 5. Research test facility for airflow measurement experiments.

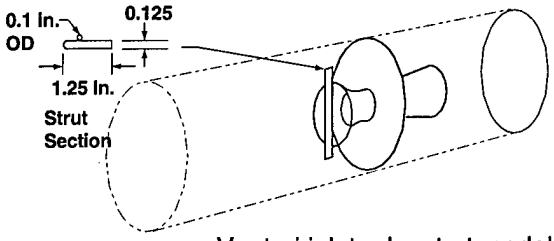

a. Venturi inlet rake strut model

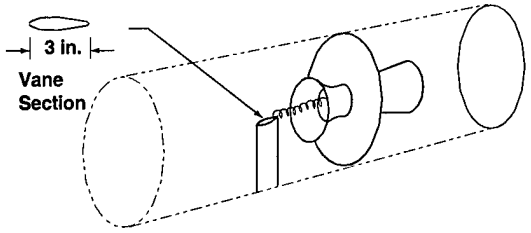

b. Vortex generator

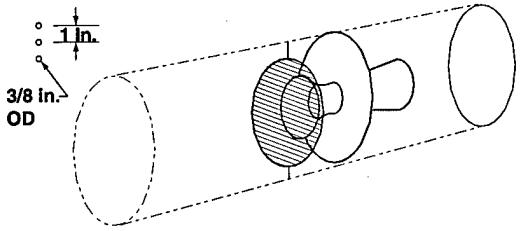

c. Turbulence Generator

Fig. 6. Flow Quality Perturbation Devices.

The primary facility instrumentation provides for the measurement of total pressure and total temperature distributions in both plenums A and B, as well as air supply and exhaust pressure. The plenum instrumentation rakes distribute probes both radially and circumferentially in the plenum cross sections (Fig. 7).

The test facility pressure tubes were routed to electronically scanned pressure transducers in order to multiplex the pressure measurements. The pressure system response characteristics were verified in laboratory bench tests prior to implementation.

Total temperature probes consisted of shielded and vented thermocouples.

Test Articles

The test articles included a family of geometrically similar venturis distinguished by throat diameter as follows:

1. A 5.64-in.-diam venturi calibrated by the flow-field probe method and used to verify the ETF database. Following calibration, the venturi served as a reference venturi in the parametric tests. This venturi was used in the baseline experiments of Ref. 5.

2. A 7-in.-diam venturi mounted in series with venturi 1 and subjected to perturbations in the test parameters for the measurement of influence coefficients.

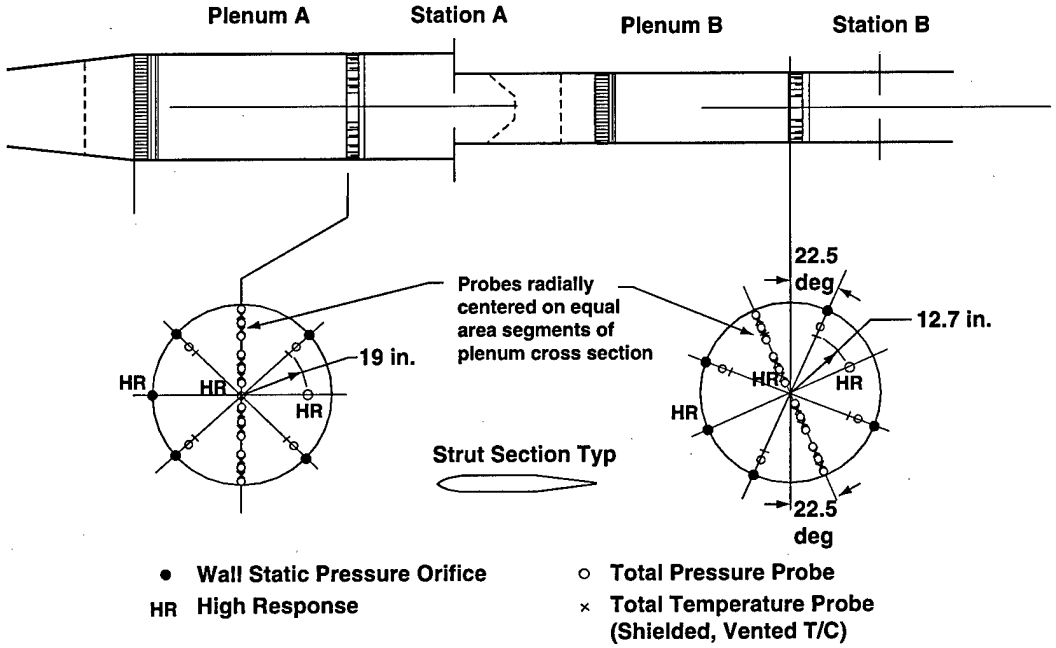

Fig. 7. Plenum chamber instrumentation.

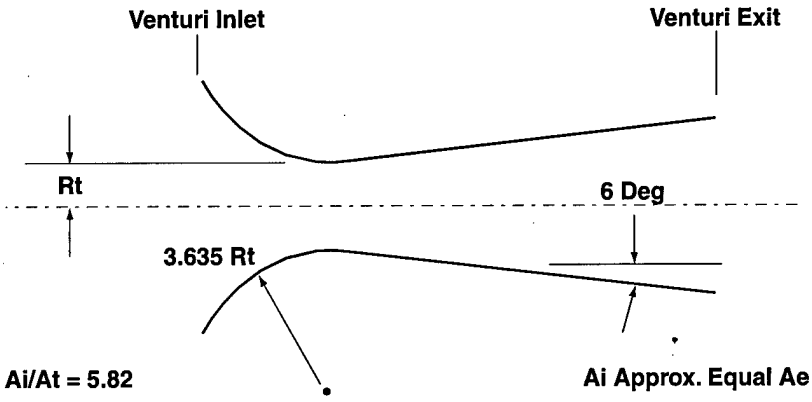

Venturi	Nom. Rt (In.)
1	2.82
2	3.50
3	5.05
4 and 5	2.50

Fig. 8. Venturi geometry.

3. A 10.1-in.-diam venturi calibrated by the flow-field probe method and used to extend the calibration throat Reynolds number and increase the boundary layer profile measurement accuracy. Following calibration, the venturi served as a reference venturi in the parametric tests.

4. Pair of 5-in.-diam venturis for tests of multiple-venturi configurations to be mounted downstream of venturi 1, and subsequently upstream of venturi 3.

Each venturi contained a circular arc contraction section followed by a conical divergent section. The circular arc contour extended from the inlet plane to a station downstream of the throat. Figure 8 provides the parameters that define the venturi configuration. Figure 9 shows venturi 1 mounted on the plenum B bulkhead with the test cell separated.

A pair of bellmouth models with diameters of 8.5 in. and 16 in., respectively, was also fabricated for the subsequent experiments directed toward the development and adoption of alternate airflow measurement methods.

The various overall test configurations available in the test apparatus appear schematically in Fig. 10. The current work includes the accomplishment of configurations 1-4 and a portion of configuration 7. The bellmouth configuration 11 tests have been completed and will appear in a subsequent report.

Each venturi contained instrumentation for the measurement of the wall static pressure distributions, high-response wall pressure, wall temperature, and boundary-layer total pressure profile. Figure 11 illustrates the venturi measurement locations. The wall static pressure orifices are located longitudinally along a ray running from the inlet to a station downstream of the throat and circumferentially around the throat station. A Kulite® high-response pressure transducer sensed fluctuating static pressure at the throat station. Chromel®/Alumel® thermocouples sensed wall temperature in the venturi contraction section and throat station as shown. The wall temperature measurements provided the material temperatures needed for thermal expansion considerations.

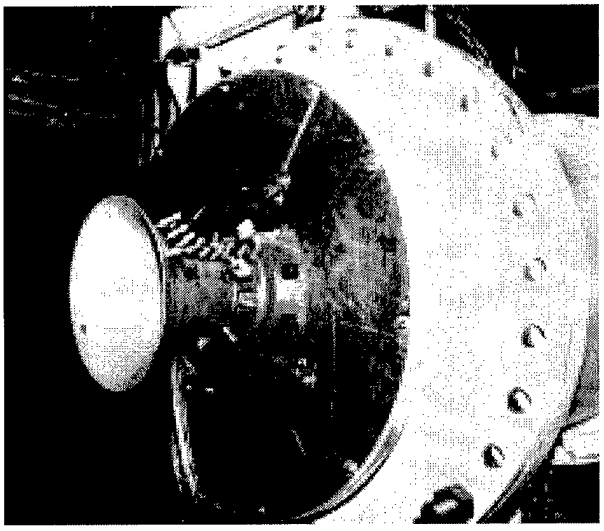

Fig. 9. Venturi 1 mounted on tet cell bulkhead.

Venturis 1 and 3 used two 10-probe rakes to measure the throat boundary-layer total pressure profiles at the 0-deg and 270-deg circumferential positions, respectively, as shown in Fig. 11. Each probe tip consists of a 0.01-in.-ID tube flattened to a 0.005-in. height for boundary-layer profile resolution purposes. The probe tip immersions were set according to the predicted boundary layer thickness for the particular venturi.

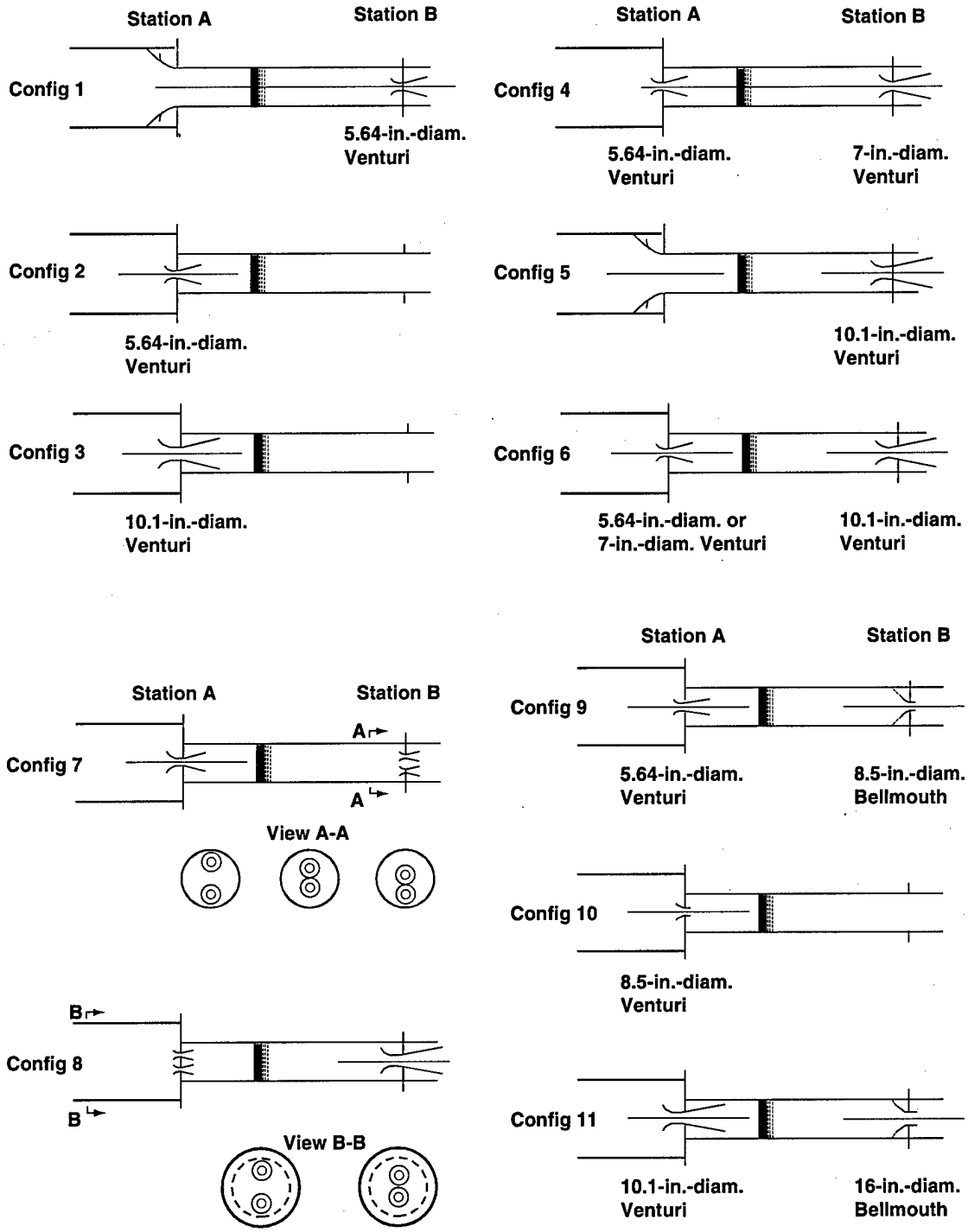

Fig. 10. General Test Configurations.

The experiment apparatus included two separate remotely controlled traversing static pressure probe systems that mount at stations A and B, respectively. The station A traversing system used an aft-facing probe that extended from a strut in the plenum through the venturi throat. The system provided the capability to traverse the throat diameter in any desired plane between the vertical and horizontal. The station B traversing system used a forward-facing traversing static pressure probe capable of traversing in the vertical plane only.

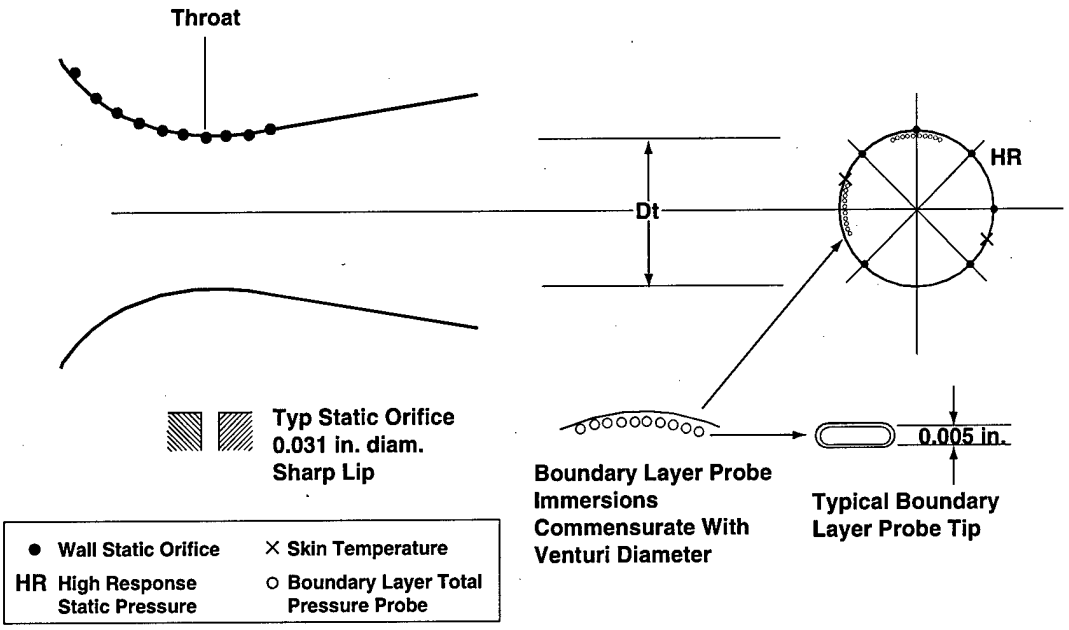

Fig. 11. Venturi instrumentation.

The configuration 1 installation used the forward-facing traversing probe system to measure the throat Mach number distribution. Shown in Fig. 12a, the probe consisted of a nominal 0.217-in.-diam body with a conical tip. A pair of 0.020-in.-diam static pressure orifices located at the 90-deg and 270-deg positions on the probe body as shown sensed the local static pressure. The configuration 1 assembly positioned the orifices at the venturi geometric throat station. The probe sting attached to a vertical strut that penetrated the exhaust duct wall and interfaced with the traversing system drive. A PC-based control system sequenced the traversing probe through a series of programmed set points.

Configurations 2 and 3 used the aft-facing probe system depicted in Fig. 12b. The aft-facing probe body and pressure orifice dimensions matched those of the forward-facing probe in the vicinity of the venturi throat. Unlike the forward-facing probe traversing mechanism, the aft-facing probe system provided two components of motion, translation, and rotation. First, the mechanism translated the probe along the diameter of the venturi throat as in the case of the forward-facing probe system. Second, the mechanism included the ability to remotely rotate the axis of translation about the venturi centerline. Thus, the system permitted traverses along any desired diameter of the venturi.

The forward-facing static pressure probe body consisted of a design that had been previously cal-

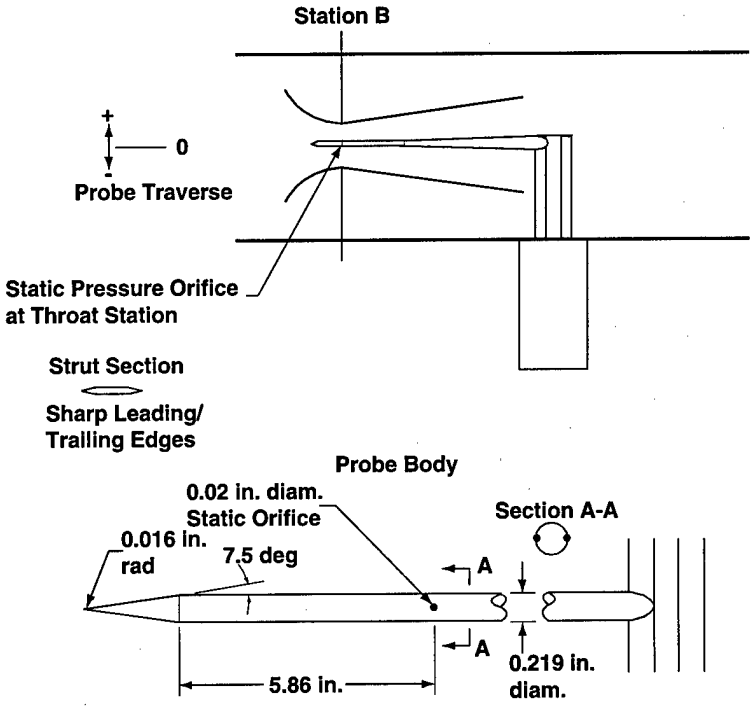

a. Forward-facing probe

Fig. 12. Traversing static pressure probes.

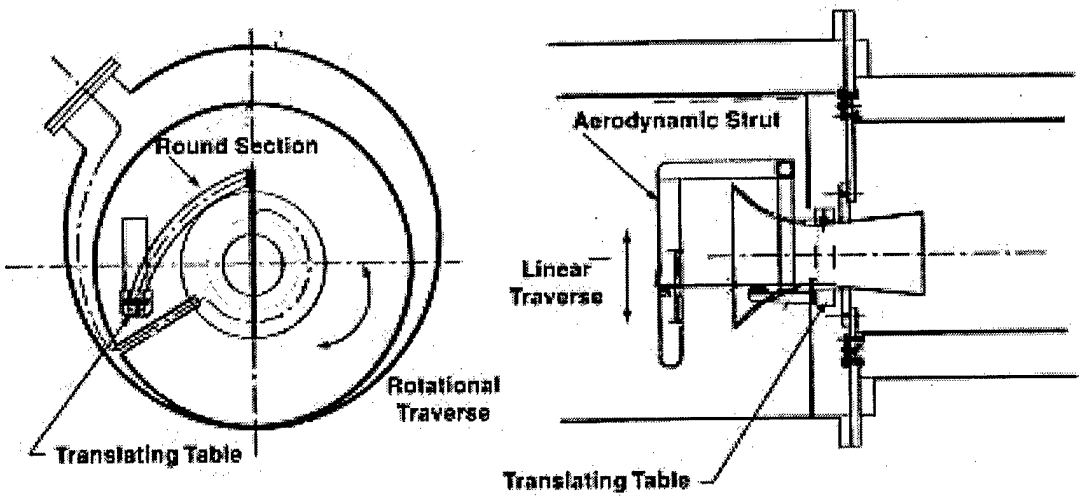

b. Aft-facing probe

Fig. 12. Concluded.

ibrated in wind tunnel tests. However, the use of the design did not totally discount the possibility of probe tip interference with the static pressure measurements. Furthermore, despite the use of an airfoil-shaped support strut located in the plenum, the potential for interference with the aft-facing static pressure probe remained a concern. Therefore, a fixed centerline static pressure pipe served as a referee for the two traversing probes. Illustrated in Fig. 13, the static pressure pipe consisted of a fixed 0.217-in.-diam probe body mounted on the venturi centerline. Four 0.020-in.-diam static pressure orifices, located as shown in Fig. 13, provided a measure of the static pressure distribution along a nominal 1-in. length. The orifices were located circumferentially in 90-deg increments around the circumference of the probe cross section to minimize the potential for aerodynamic interference between orifices. To minimize tip interference, the centerline static pressure pipe mounted with the tip upstream of the venturi inlet plane. Four stainless steel wires supported the tip with minimal plenum flow interference. The downstream end of the pipe mounted to a strut in the exhaust duct, downstream of the venturi divergent section.

The probe miniaturization required to resolve the boundary-layer and throat pressure profiles adversely affects the pressure measurement system response characteristics. Unlike the facility

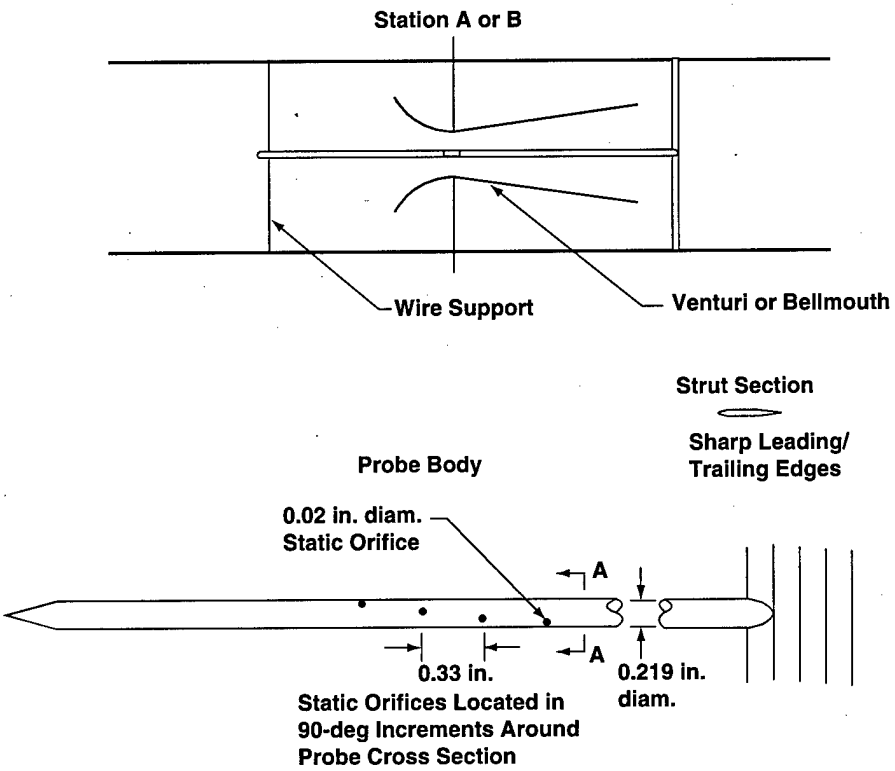

Fig. 13. Centerline static pressure pipe.

pressure measurements, the boundary-layer and throat static pressure distribution measurements required special provisions to achieve acceptable system response. The instrumentation system included a remote pressure module rack located adjacent to the test cell instead of inside the control room. The boundary-layer probes, traversing static pressure probes, and the centerline static pressure pipe were connected to the remote pressure modules with the lengths of the pressure tube runs maintained below 10 feet. Furthermore, each of the three types of probes used a unique pressure tube diameter selected, based on the results of laboratory tests of the system response.

Test Procedure

The scope of the objective 1 experiments, configurations 1-4, encompassed the following overall test procedures: (1) centerline static pressure pipe tests, (2) throat static pressure survey tests, (3) boundary layer survey tests, and (4) tandem venturi tests. The first three procedures applied to each of the first three test configurations. The fourth procedure applied to the parametric tests under configuration 4. The primary test condition variable was the throat Reynolds number, the Reynolds number based on throat diameter. Throat Reynolds number varied from 0.4E6 to 10.5E6, spanning a range of laminar, transitional, and turbulent throat boundary-layer conditions. The authors of Ref. 5 noted that the Reynolds numbers below approximately 0.7E6 yielded predominantly laminar flow in the contraction section boundary layer. Flows with Reynolds numbers in the range of 0.7E6 to 2.7E6 were characterized by boundary layers in transition from laminar to turbulent. A fully turbulent boundary layer characterized conditions with Reynolds numbers over 2.7E6.

The test conditions were established by setting TT = 530 R and adjusting PTINF according to the required throat Reynolds number. This selection of TT matched the laboratory conditions maintained during the measurement of venturi throat radius, Rt, eliminating the need to account for material thermal expansion or contraction effects.

During the execution of each procedure, pressure module ranges were adjusted to help manage pressure measurement errors. This entailed dividing the test conditions into three groups corresponding, respectively, to low-range pressure, mid-range pressure, and high-range pressure. Matching pressure transducer range to pressure measurement range required physically switching pressure modules during the course of a test period.

The centerline static pressure pipe test procedure involved establishing each test condition and recording five repeat data points. Simultaneously, the boundary-layer rakes provided boundary-layer total pressure profiles.

The venturi throat static pressure survey tests focused on traverses of the throat diameter using the forward-facing probe system (configuration 1) or the aft-facing probe system (configurations 2 and 3). Each survey consisted of 17 probe positions spanning the venturi diameter. The procedure included a pause at each probe position for pressure system stabilization and data point recording. High-response data were recorded on analog tape when the probe traverse reached the venturi centerline. Traverses in the opposite direction provided repetition of selected points. The configuration 1 surveys included traverses along the vertical line of symmetry in the throat cross section. The variability roll capability of the aft-facing probe mechanism provided corresponding surveys along lines at additional roll angles of 45 deg, 90 deg, and 135 deg to more completely map the cross section. The data system also recorded the boundary-layer total pressure measurements in conjunction with each static pressure measurement on the traverse.

The test matrix for configurations 1-3 appears in Fig. 14. The configuration 3 portion of the matrix, involving the 10.1-in.-diam venturi, required adjustment of the total pressure to match the configuration 1 and 2 Reynolds numbers. By virtue of the larger throat diameter, configuration 3 also permitted an extension of the Reynolds number beyond configurations 1 and 2 at the higher pressure conditions.

Although the throat static pressure survey tests yielded boundary-layer measurements as well, the test procedures included boundary-layer tests as

separate entities. Dedicated to the boundary layer, the tests were conducted with the traversing static pressure probes and the centerline static pressure pipe absent to provide a data set free from any possibility of static pressure probe interference. Sets of repeat boundary layer measurements were obtained at each test condition.

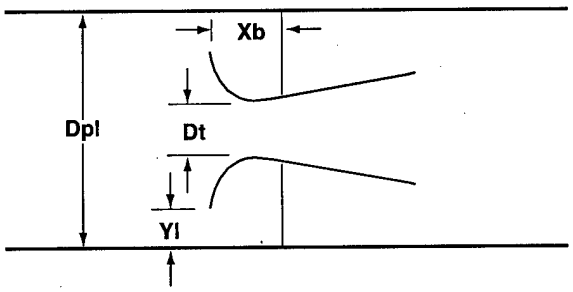

Configuration	Xb/Dt	Dpl/Dt	Yl/Dt	REY, millions
1	1.95	6.383	1.986	0.40, 0.68, 0.85, 1.03, 1.33, 2.71, 4.11, 5.45
2	1.95	9.57	3.58	0.40, 0.68, 0.85, 1.03, 1.33, 2.71, 4.11, 5.45
3	1.25	5.347	1.49	0.68, 0.85, 1.03, 1.33, 1.85, 2.71, 4.11, 5.45, 7.73, 10.50

Fig. 14. Configurations 1-3 test matrix.

The tandem venturi tests, configuration 4, relied on comparisons between the test venturi and the reference venturi for determining the effect of parametric variations on the former. The procedure started with establishing the baseline test venturi flow coefficient relative to the reference venturi. The baseline configuration consisted of the test venturi positioned on the plenum centerline with the venturi inlet plane 1.95 throat diameters upstream of the bulkhead. The baseline plenum was devoid of all flow perturbation devices to provide uniform conditions. The reference venturi flow rate normalized by the test venturi flow rate yielded a measure of the differences prior to perturbation of parameters. Subsequently, various installation and flow quality parameters were systematically perturbed and changes in the differences measured.

The installation parameters varied included the spacing between the venturi inlet and the bulkhead and the spacing between the venturi lip and the plenum wall (coupled with the introduction of an asymmetry due to the offset venturi position). An additional installation parametric test included the pair of 5-in.-diam venturis mounted in the closest proximity position. Flow quality parameters included the total pressure profile, swirl, and turbulence. With respect to flow quality, this initial study did not include a detailed mapping of the flow field produced at the venturi inlet by each of the devices. Rather, overall flow perturbations representative of those expected in the full-scale facilities were used for screening with the intention of identifying for detailed study those of significance. The test matrix appears in Fig. 15. Repeat data points were recorded at each perturbed configuration or condition in the matrix. The matrix depicted in Fig. 15 represents a somewhat abridged version of the original matrix. Planned geometric variations such as surface roughness and venturi contraction ratio were cancelled due to budgetary considerations and a shift in emphasis toward the bellmouth development.

Data Analysis and Uncertainty

The primary configurations 1-3 data analyses focused on comparing the present results with the historical data presented in Ref. 5. The comparisons included the boundary-layer total pressure profiles, throat Mach number distributions derived from the throat static pressure traverses, and the venturi flow coefficient. The venturi flow coefficient resulted from the integration of the boundary layer for displacement thickness and the integration of the core mass flux distribution.

The analysis of configuration 4 results focused on determining the effect of the test parameter perturbations on test venturi flow coefficient. The parameter CF DEV simplified the comparisons by removing biases in the baseline data:

$$\text{CF DEV} = |(\text{CFBA-1 of test case}) - (\text{CFBA-1 baseline})| / \text{CFBA-1 baseline}$$

The complete assessment of the measurement uncertainty is in preparation in conjunction with the

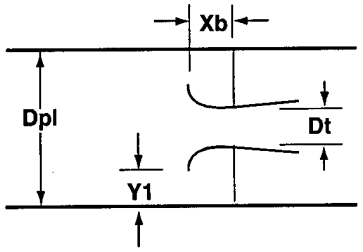

Category	Parameter	Xb/Dt	Dpl/Dt	Yl/Dt	REY, millions	Comment
Baseline	Baseline	1.950	5.143	1.366	0.68, 0.85, 1.03, 1.33, 2.71, 4.11, 4.69	
Installat.	Inlt.-Bulk Spac	0.95	5.143	1.366	Same sequence of test conditions used for all perturbations.	
	Inlt-Bulk Spac	0.00	5.143	1.366		
	Lip-Wall Spac	0.00	5.143	0.58		
Flow Qual.	Tot Pres Prof	1.950	5.143	1.366		Simul Instr Rake
	Swirl	1.950	5.143	1.366		Swirl Gen Vane
	Turbulence	1.950	5.143	1.366		Turb Generator

Fig. 15. Configuration 4 test matrix.

data analysis. However, the initial assessments yielded the following uncertainty estimates:

PT/PTINF: +/- 0.002 max

MACH: +/-0.003

CF DEV: +/- 0.0006

Y: +/- 0.003 in.

Results

Boundary-Layer Total Pressure Profiles

A number of boundary-layer total pressure profile comparisons between the present configuration 1 experiments and the Ref. 5 experiments appear in Fig. 16. Figure 16 displays plots of local total pressure versus probe immersion. The lines represent the original curve fits of the 1961 data set. The symbols represent a portion of the present measurements. Figure 16a provides a comparison at the laminar Reynolds number of 0.68E6. In both the 1961 and 1996 experiments the thin laminar boundary layer enclosed only a portion of the boundary-layer probes. However, the figure illustrates the relatively good agreement between the data sets. Figure 16b shows a similar comparison at a transitional Reynolds number condition. In this case, a significant portion of the flow upstream of the throat was laminar. On this particular test point, the top-mounted rake measured a profile closer to a laminar shape than the side-mounted rake. As a result, the side-mounted rake results provided a closer agreement to the profile reported in Ref. 5, and the top-mounted rake yielded a steeper profile. Finally, Fig. 16c provides a comparison at a turbulent Reynolds number. The plot clearly displays the turbulent character of the total pressure profile shape and the considerably thicker boundary layer. Again, the present results compared well with the 1961 baseline.

Core Flow Mach Number Distributions

Local throat core flow static pressure measurements from the traversing probe and plenum total pressure measurements provided the core flow Mach number distributions. A typical profile spanning the throat diameter from the bottom wall to the top wall appears in Fig. 17. The figure displays the distribution on a plot with the Mach number as the ordinate and the probe position, normalized by throat radius, as the abscissa. The plot includes results from the 1961 experiments, and the present configuration 2 and 3 experiments, as well as the series solution of the core flow used in the current flow coefficient calculation.[6] The present Mach

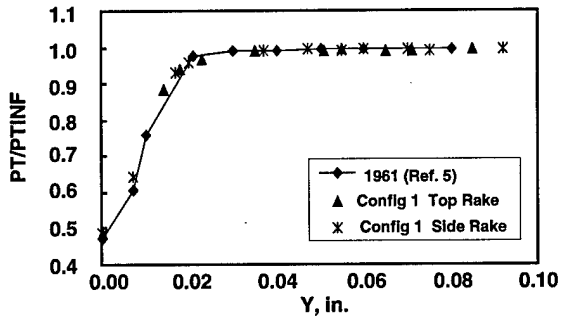

a. Laminar Reynolds Number of 0.68E6

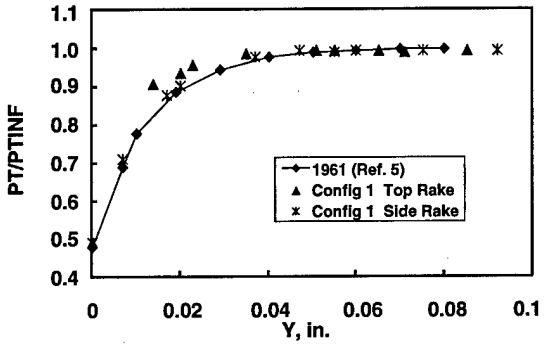

b. Transitional Reynolds Number of 1.33E6

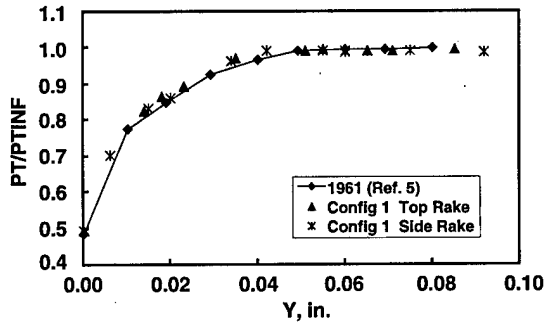

c. Turbulent Reynolds Number of 2.71E6

Fig. 16. Comparison of venturi throat boundary layer total pressure profiles.

number profile agreed reasonably well with the Smith and Matz profile. However, the present measurements displayed a more symmetrical profile with respect to the venturi axis. The analytical solution differed slightly from both experimental profiles as shown.

Throat Mach number distributions measured in configuration 3 tests spanning a range of Reynolds numbers appear in Fig. 18. Configuration 3 provided the widest range of Reynolds number in the present tests. The plots display the agreement between the 1961 and the present experiments at laminar, transitional, and turbulent Reynolds numbers. Smith and Matz reported a weak Reynolds

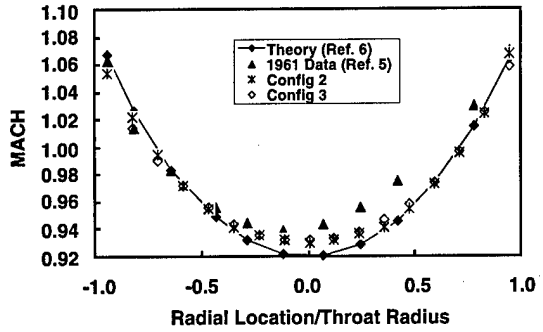

Fig. 17. Venturi throat core flow Mach number distribution comparison.

number dependence in the Mach number distributions.[5] The present distributions also varied slightly with Reynolds number as shown.

The differences between the analytical solution used in the ETF flow coefficients and the 1961 measurements were larger than the differences between the present measurements and the analytical solution. This result, in conjunction with the insensitivity to the Reynolds number, helps substantiate the consistency between the historical theoretical curve and the flow coefficient accuracy. The observed differences will become a subject in the accuracy assessment and improvement work.

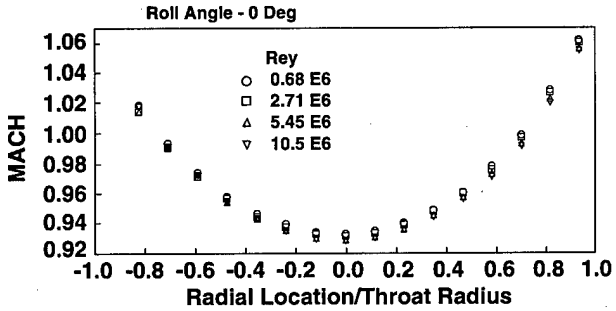

Fig. 18. Venturi throat Mach number distribution variation with Reynolds number - configuration 3.

Venturi Flow Coefficients

Comparisons of the venturi flow coefficients between the Smith and Matz experiments and the present experiments appear in Fig. 19. The figure includes a plot of discharge coefficient as a function of throat Reynolds number. The plot displays the excellent agreement between the present and historical data at the turbulent Reynolds numbers. At the laminar Reynolds numbers the data also

agreed well, although the differences were slightly larger. Both data sets deviated somewhat from the theoretical curve that forms the basis for the currently used coefficients. The theoretical curve depicted in Fig. 19 used the method of Ref. 6 for the streamline curvature component of Cd and the method of Ref. 7 for the boundary-layer component. The deviation shown in Fig. 19 suggests that the models used to characterize Cd in the airflow data reduction algorithms offer opportunities for accuracy improvement.

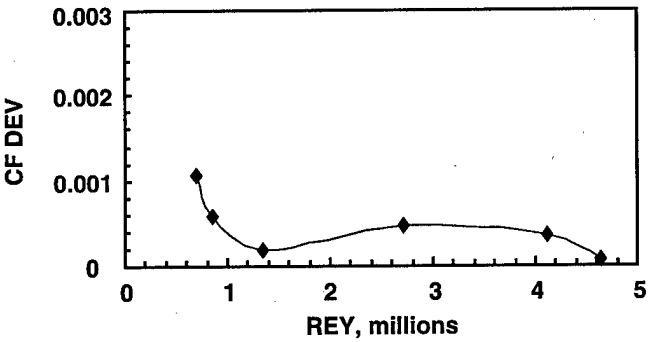

Fig. 20. Initial baseline test compared to repeat baseline test.

The venturi flow coefficient comparisons, in conjunction with the boundary-layer total pressure profile comparisons and core flow Mach number profile comparisons, substantiated the 1961 data set that form the basis for the currently used algorithms. As a result, the experiments addressed the initial issues raised under objective 1 of the study. The next set of results begins the process of assessing the venturi airflow measurement accuracy when installed in ETF facilities.

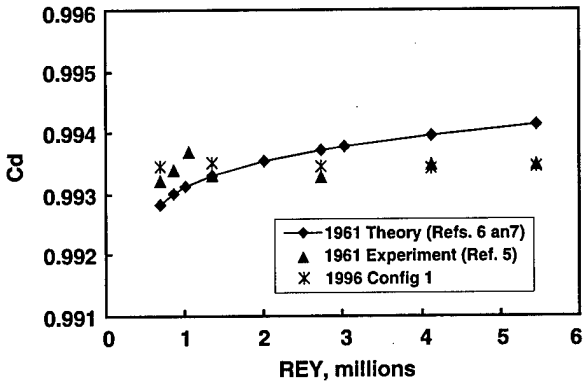

Fig. 19. Venturi flow coefficient comparisons.

Influence of Installation and Flow Quality Parameters

The configuration 4 baseline tests provided a measure of the bias between the test venturi and the reference venturi. In addition, the repeat points substantiated the pretest prediction of the data precision. During the course of the baseline testing, conditions from one test period were repeated on a subsequent test period to capture any effects induced by test shutdown and test startup procedures. A comparison of the results from two such baseline tests appears in Fig. 20 in terms of CF DEV. The figure shows that over most of the Reynolds number range, the two baseline tests agreed to within 0.0005, consistent with predicted precision in CF DEV. At the lowest Reynolds number, low-pressure conditions where laminar boundary-layer characteristics dominate, the deviation increased to 0.001. These results provided a measure of the resolution in the data and the limit on the ability to discern between the perturbation parameter effects and data precision effects. As deviations on the order of 0.0006 may be attributed to data uncertainty, deviations below 0.0006 were classified as inconclusive with respect to the effect of a perturbation on flow coefficient.

The use of both freestanding venturi installations (venturi inlet plane upstream of bulkhead) and flush venturi installations (venturi inlet plane flush with bulkhead) in ETF facilities elevated the spacing between the venturi inlet plane and the bulkhead as a key installation parameter. As the baseline configuration consisted of the freestanding venturi with Xb/Dt = 1.95, the perturbations consisted of a flush installation with Xb/Dt = 0 and an intermediate spacing with Xb/Dt = 0.95. The effect of the perturbation to the flush installation appears in Fig. 21. Such a configuration typifies an ETF Test Cell T-2 or T-4 venturi installation. Over the turbulent range of Reynolds numbers, the change in spacing raised CF DEV to approximately 0.0008. Thus, the bulkhead spacing change induced a relatively small but measurable change in flow coefficient. Although not shown here, the intermediate inlet-to-bulkhead spacing yielded a CF DEV between the 0.0005 baseline variation and the 0.0008 flush case over the range of turbulent Reynolds numbers. Thus, the spacing between the bulkhead and the venturi inlet plane

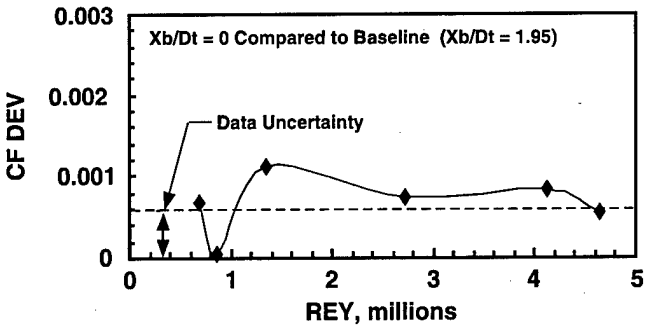

Fig. 21. Effect of spacing between venturi inlet plane and bulkhead on flow coefficient.

apparently represents a variable with some influence on the airflow measurement accuracy. As the parameter is currently neglected as a variable in the venturi data reduction algorithms, it contributes to airflow rate uncertainty. Therefore, future accuracy improvements will consider accounting for the effect either by including the bulkhead spacing in the flow coefficient models or by specifying a particular spacing for all installations.

The introduction of an offset between the venturi centerline and the plenum centerline produced a more pronounced installation effect than the bulkhead spacing. The test entailed repositioning the venturi to decrease the spacing between the venturi inlet lip and the plenum wall. The apparatus provided a spacing corresponding to YI/Dt = 0.58. The offset also introduced an asymmetry in the geometry and, therefore, an asymmetry in the flow path between the plenum and the venturi entrance. The results shown in Fig. 22 included CF DEV levels on the order of 0.004 over the range of turbulent Reynolds numbers. The results indicated that either the asymmetry, the interaction between the venturi lip and the plenum wall, or a combination of the two contributed significantly to a change in flow coefficient. As a result, the screening identified the offset installation for consideration in the accuracy improvement work.

The total pressure distribution generated in the wake of an instrumentation rake such as those installed in a number of the Aeropropulsion Systems Test Facility (ASTF) test cell C-1 and C-2 venturis was simulated directly by using the geometrically scaled rake simulator mounted at the venturi inlet. The results appear in Fig. 23. Although the variation in CF DEV over the range of turbulent Reynolds numbers may have changed shape, the magnitude was generally indistinguishable from the data precision. This result suggested that the wake produced by the instrumentation rake contributed little to the flow coefficient and may be neglected in the accuracy improvement work.

The introduction of localized swirl, using the tip vortex produced by the vane, yielded the results shown in Fig. 24. As in the case of the instrumentation rake wake, the level in CF DEV was sufficiently low to be indistinguishable from the data precision. This result suggested that low lev-

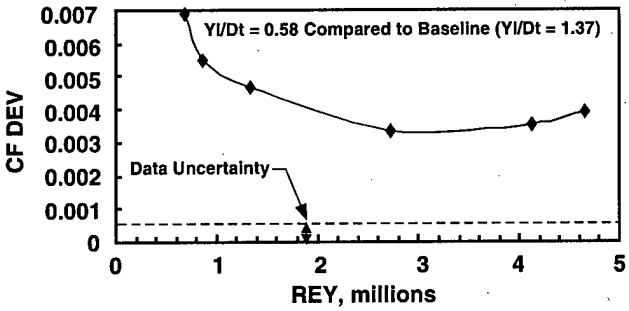

Fig. 22. Effect of Venturi lateral offset on flow coefficient.

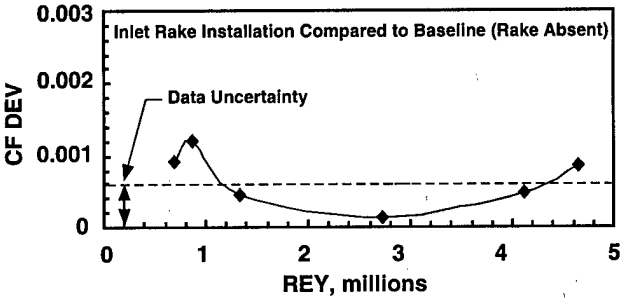

Fig. 23. Effect of flow quality perturbation produced by inlet rake on flow coefficient.

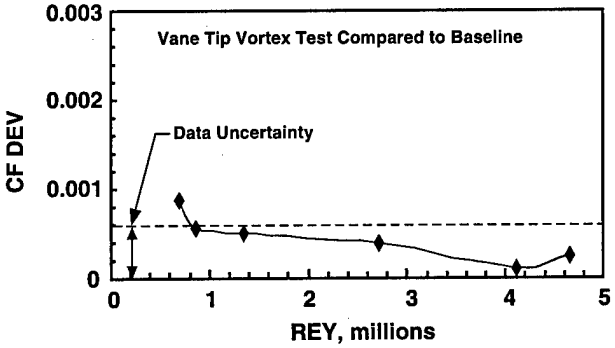

Fig. 24. Effect of local swirl on flow coefficient.

els of localized swirl would have a negligible effect on the flow coefficient. As a result, subsequent tests with swirl were deferred.

Conclusions and Recommendations

The results yielded the following conclusions:

1. The venturi boundary-layer total pressure measurements substantiate the results reported in Ref. 5, including profiles characteristic of predominantly laminar, transitional, and turbulent conditions.

2. At transitional Reynolds numbers, the boundary-layer profile may vary in shape with circumferential location in the throat cross section.

3. The throat core flow Mach number measurements substantiate the distributions reported in Ref. 5.

4. When integrated, the boundary layer and core flows yielded flow coefficients that agreed with the Ref. 5 baseline data. Therefore, the data set that forms the basis for the current ETF algorithms is valid.

5. Variations in the venturi installations affect the flow coefficient. The flow coefficient is relatively insensitive to the spacing between the venturi inlet plane and the bulkhead. However, the spacing between the venturi lip and the plenum wall, in conjunction with the asymmetry, significantly affected the flow coefficient.

6. The venturi flow coefficient is insensitive to small variations in total pressure, as well as small regions of localized swirl.

7. The differences between the experiment and the theoretical models offer the opportunity for accuracy improvement through improved computational models.

The current data set achieved the goal of verifying the historical database and the current flow coefficient algorithms. It also provided an initial screening of flow coefficient sensitivities to a number of installation and flow quality parameters. However, changes in budgetary constraints and investment strategies resulted in a significant reduction in test scope. As a result, the current data set excludes a number of parametric variations and measurements necessary to establish the flow coefficient sensitivities fully. Furthermore, the application of sensitivity measurements to the full-scale accuracy assessment requires detailed measurements of the parameter variations in the test cells. Recommendations for future work include the following:

1. Complete screening tests to address geometric and installation parameters currently omitted. These include such parameters as surface roughness, machining imperfections, venturi contraction ratio, multiple-venturi spacing, and Dt/Dpl.

2. Investigate the increment in flow coefficient produced by the lateral offset in venturi position. Determine relative effects of plenum wall proximity and the asymmetry.

3. Based on the screening test results, map the plenum and venturi inlet flow fields in terms of flow angularity, pressure variations, and turbulence in both the subscale and full-scale facilities.

4. Apply the sensitivity results in the installed accuracy and accuracy improvement studies. For each parameter significantly influencing airflow, improve accuracy either by accounting for the sensitivity in the calibration or by specifying an allowable range in the parameter.

The current plan for the future focuses on the development of the bellmouth as the airflow measurement standard in the ETF facilities. The motivation for the emphasis on the bellmouth method is the potential for a substantial reduction in the cost of test operations at the ETF. Toward this end, the configuration 11 bellmouth experiments have been completed. Analysis of the experimental results and a parallel development of needed CFD tools are in progress.

References

1. Bartlett, C. R. and Turner, E. E., "Performance Evaluation Methods for the High-Bypass-Ratio Turbofan," AIAA Paper No. 75-1206, AIAA/

SAE 11th Propulsion Conference, Anaheim, CA, September 1975.

2. Smith, R. E., Jr. and Wehofer, S., "Measurement of Engine Thrust in Altitude Ground Test Facilities," AIAA Paper No. 82-0572, AIAA 12th Aerodynamic Testing Conference, Williamsburg, VA, March 1982.

3. Reed, J. A., Hiers, R. S., Jr. and Turrentine, W. A., Jr., "Improvement of Flow Quality in Turbine Engine Test Cells by the Elimination of Bellmouth-Induced Core-Flow Vortices," AIAA Paper No. 2391, 33st AIAA/ASME/SAE/ASEE Joint Propulsion Conference and Exhibit, San Diego, CA, July 1995.

4. De Siervi, F., Viguier, H. C., Greitzer, E. M., and Tan, C. S., "Mechanisms of Inlet-Vortex Formation," *Journal of Fluid Mechanics*, Vol. 124, 1982, pp 173-207.

5. Smith, R. E. and Matz, R. J., "Verification of a Theoretical Method of Determining Discharge Coefficients for Venturis Operating at Critical Flow Conditions," Transactions of the ASME, December, 1962.

6. Oswatitsch, K. and Rothstein, W., "Flow Pattern in a Converging-Diverging Nozzle," NACA TM 1215, March 1949.

7. Tucker, M., "Approximate Calculation of Turbulent Boundary Layer Development in Compressible Flow," NACA TN 2337, April 1951.